ACKNOWLEDGMENT

The authors are indebted to B. Loriou, M. Goloubkoff, and Y. Garnier for their assistance in performing this study.

REFERENCES

[1] Schneider, "Millimeter-wave integrated circuits," in *IEEE Int. Microwave Symp. Digest* (Univ. of Colorado, Boulder), June 4–6, 1973.
[2] F. Z. Keister, "An evaluation of materials and processes for integrated microwave circuits," *IEEE. Trans. Microwave Theory Tech.*, vol. MTT-16, pp. 469–475, July 1968.
[3] M. Caulton, "Film technology in microwave integrated circuits," *Proc. IEEE*, vol. 59, pp. 1481–1489, Oct. 1971.
[4] H. Sobol, "A review of the technological and electromagnetic limitations of hybrid circuits for microwave applications," *IEEE. Trans. Parts, Hybrids, Packag.*, PHP-8, pp. 59–66, June 1972.
[5] R. A. Pucel *et al.*, "Losses in microstrip," *IEEE. Trans. Microwave Theory Tech.*, vol. MTT-16, pp. 342–350, June 1968.
[6] Joly, "Lignes Télégraphiques et Téléphoniques." France. Private communication.
[7] J. Magarshack, "Laboratoire de Physique Appliquée," France, private communication.
[8] T. T. Hitch *et al.*, "Chemical analyses of thick film gold conductor inks," *IEEE. Trans. Parts, Hybrids, Packag.*, vol. PHP-11, pp. 248–253, Dec. 1975.
[9] Horton *et al.*, "Variation of microstrip losses with thickness of strip," *Electron. Lett.*, vol. 7, 1971.
[10] M. Goloubkoff, "Rélaisation en microélectronique d'un amplificateur à transistors hyperfréquences en bande *L*," Symposium Microelektronik 5 Munich–Novembre 1972.
[11] E. J. Crescenzi *et al.*, "Fused silica A better substrates for mixers," *Microwaves*, Jan. 1976.
[12] V. S. Aramati *et al.*, "Thin-film microwave integrated circuits," *IEEE Trans. Parts, Hybrids, Packag.*, vol. PHP-12, pp. 309–316, Dec. 1976.

A Generalized Spectral Domain Analysis for Coupled Suspended Microstriplines With Tuning Septums

TATSUO ITOH, SENIOR MEMBER, IEEE, AND ALBERT SIDNEY HEBERT, MEMBER, IEEE

Abstract—**An efficient computation method is developed for solving the microstrip-type structures in which a number of conducting strips are located on several interfaces of dielectric layers. The method is applied to the coupled suspended microstripline with tuning septums on the underside of the suspending dielectric layer. The numerical solutions obtained by the new method are compared with available data. The method is believed useful in the design of tightly coupled structures such as the 3-dB hybrid as well as of transitions between different transmission lines for microwave and millimeter-wave integrated circuit application.**

I. INTRODUCTION

THIS PAPER describes a new efficient method for computing characteristic impedances and effective dielectric constants of the even and odd modes in the coupled suspended microstriplines with grounded tuning septums. The cross section of the structure is shown in Fig. 1. This structure recently has been introduced by Aikawa [1], [2] to circumvent some of the practical difficulties in realizing coupled microstripline structures such as a 3-dB hybrid.

Manuscript received November 11, 1977. This work was supported in part by a U. S. Army Research Grant DAAG29-77-G-0220.

The authors are with the Department of Electrical Engineering, University of Kentucky, Lexington, KY 40506.

It is well known that the phase velocities or the effective dielectric constants of the even and odd modes must be identical or close to each other within a few percent in order that the coupled microstripline structure can be used as a directional coupler. In addition, the separation $2S$ between two strips must be reasonably large so that the structure can be fabricated without undue practical difficulty. Several methods have been reported to control the phase velocities of the even and odd modes and to realize a tightly coupled structure. They include the dielectric overlay [3], the wiggly line [4], and the interdigitate line [5].

In the method proposed by Aikawa [2], the value of $2S$ to obtain a tight coupling is relatively large, and the phase velocity of the even mode can be tuned by changing the width of the grounded septums. It is also pointed out that the proposed structure is potentially useful as a reverse phase hybrid ring [1]. We also believe this structure is useful at millimeter-wave frequencies because it is a modification of the suspended microstripline [6].

The analysis of the structure has been done by the use of the successive over-relaxation technique [1], [2]. In this paper, an alternative and very efficient numerical technique is developed for analyzing the structure shown in

0018-9480/78/1000-0820$00.75 ©1978 IEEE

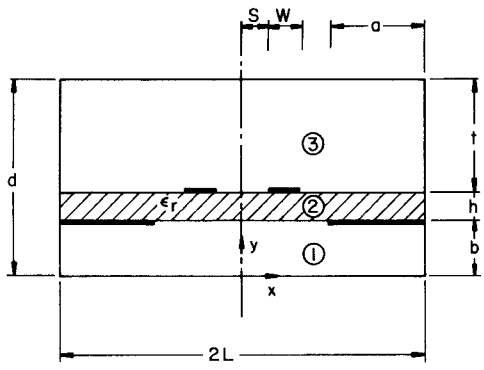

Fig. 1. Cross section of coupled suspended lines with septums.

Fig. 1. The method is essentially a generalization of the spectral domain technique developed by Itoh and Mittra for solving a number of microstripline structures [7]–[9]. However, the original version of the technique is applicable only to the structures in which strips or slots are located on one of the interfaces between different dielectric regions. In the generalized version presented here, the above restriction is no longer required, and we can analyze the structures in which strips and/or slots are located at various interfaces. Although in this paper only the structure in Fig. 1 is analyzed, the new method itself is quite general and can be applied to a number of microstrip type structures that contain several strips located on more than one interface between dielectric layers.

The method in this paper has a number of attractive features. 1) The method is numerically simpler and more efficient than many conventional space-domain analyses such as the finite difference techniques. This is due primarily to the fact that, in the present method, solutions are extracted from algebraic equations rather than from coupled integral equations or differential equations typically appearing in the conventional space-domain approaches. 2) The use of Fourier transforms allows one to convert convolution integrals into algebraic products, thus avoiding the necessity of numerical evaluation of complicated integrals, a process which is often extremely time consuming. 3) Unlike many other methods, the physical or qualitative nature of the field corresponding to the modal solutions is directly incorporated in the process of solution via the appropriate choice of basis function as described later. 4) The solution by this method is stationary in nature. This means that the computed characteristic impedances of even and odd modes are insensitive to the first-order error associated with the basis functions. 5) The accuracy of the solution can be improved systematically by increasing the size of the matrix associated with the system of linear equations. However, the matrix size required for accurate solutions is typically 2×2 or 4×4 and is much lower than the one to be used in many other methods. 6) The coupling phenomena between strips and septums will appear in the solution process in a form clearly identifiable. In the next two sections, the formulation process will be presented, and the solution method given. Only the important steps will be described. In Section IV some numerical results will be presented and compared with other available data.

II. Formulation of the Problem

In this paper we will restrict ourselves to cases where the quasi-TEM approximation is valid, although the present method can easily be extended to a more rigorous dispersion analysis. Under this assumption, we only need to solve Poisson's equation in the cross section subject to appropriate boundary conditions and to obtain line capacitances for both even and odd modes. From these quantities, characteristic impedances and the normalized guide wavelengths (or, equivalently, the effective dielectric constants) of these modes can be readily obtained.

Since the structure in Fig. 1 is symmetric with respect to the y axis, we need to consider only the right-hand half ($0<x<L$) after placing either a magnetic or an electric wall for the even and odd mode, respectively. When we designate three regions, $0<y<b$, $b<y<b+h$, and $b+h<y<d$, with the index $i=1$, 2, and 3, the interface conditions to be satisfied are

$$\phi_1(x,b)=\phi_2(x,b), \qquad 0<x<L \tag{1a}$$

$$\phi_1(x,b)=\begin{cases} 0, & L-a<x<L \text{ (on septum)} \\ v(x), & 0<x<L-a \end{cases} \tag{1b}$$

$$\epsilon_r \frac{\partial\phi_2}{\partial y}\bigg|_{y=b} - \frac{\partial\phi_1}{\partial y}\bigg|_{y=b} = \begin{cases} -\dfrac{\rho_s(x)}{\epsilon_0}, & L-a<x<L \text{ (on septum)} \\ 0, & 0<x<L-a \end{cases} \tag{1c}$$

$$\phi_2(x,b+h)=\phi_3(x,b+h), \qquad 0<x<L \tag{2a}$$

$$\phi_2(x,b+h)=\begin{cases} V, & S<x<S+W \text{ (on strip)} \\ \phi_0(x), & 0<x<S, S+W<x<L \end{cases} \tag{2b}$$

$$\frac{\partial\phi_3}{\partial y}\bigg|_{y=b+h} - \epsilon_r \frac{\partial\phi_2}{\partial y}\bigg|_{y=b+h} = \begin{cases} -\dfrac{\rho(x)}{\epsilon_0}, & S<x<S+W \text{ (on strip)} \\ 0, & 0<x<S, S+W<x<L \end{cases} \tag{2c}$$

where $\phi_i(x,y), i=1,2,3$ are potential functions in Region i, ϵ_r is the relative dielectric constants of the dielectric slab, V is the known potential of the strip, and ϵ_0 is the free space permittivity. $\rho_s(x)$ and $\rho(x)$ are unknown charge distributions on the septum ($L-a<x<L, y=b$) and on the strip ($S<x<S+W, y=b+h$), respectively. On the other hand, $v(x)$ and $\phi_0(x)$ are unknown potential distributions as the respective interfaces. In addition $\phi_i(x,y)$ must be zero on the conducting peripheral walls and $\phi_i(0,y)=0$ or $(\partial\phi_i(0,y))/(\partial x)=0$ on the electric or magnetic wall at $x=0$.

Instead of solving the two-dimensional static problem in the space (x,y) domain, we will work in the Fourier transform or spectral domain. To this end we will introduce finite Fourier transforms via

$$\tilde{\phi}(n,y)=\int_0^L \phi(x,y)\cos \hat{k}_n x\,dx,$$

$$\hat{k}_n=\frac{n-1/2}{L}\pi \quad n=1,2,\cdots \tag{3a}$$

$$\tilde{\phi}(n,y)=\int_0^L \phi(x,y)\sin \hat{k}_n x\,dx,$$

$$\hat{k}_n=\frac{n}{L}\pi \quad n=1,\ 2,\cdots \tag{3b}$$

where (3a) is for the even mode whereas the odd mode requires the use of (3b). This distinction is due to the different symmetry conditions at $x=0$ for these two orthogonal modes. Also these choices of the transform variables $\hat{k}_n$ assure that $\phi(L,y)=0$ for both even and odd modes. When Fourier transformed, the Laplace equation for ϕ becomes

$$\frac{d^2\tilde{\phi}}{dy^2}-\hat{k}_n^2\tilde{\phi}=0. \tag{4}$$

The rest of the formulation process in the remainder of this section remains identical for both even and odd modes. The solutions of (4) in each region are

$$\tilde{\phi}_1(n,y)=A_n \sinh \hat{k}_n y \tag{5}$$

$$\tilde{\phi}_2(n,y)=B_n^s \sinh \hat{k}_n(y-b)+B_n^c \cosh \hat{k}_n(y-b) \tag{6}$$

$$\tilde{\phi}_3(n,y)=C_n \sinh \hat{k}_n(d-y) \tag{7}$$

where A_n, B_n, and C_n are unknown coefficients to be determined. Notice that $\tilde{\phi}_1(n,0)=\tilde{\phi}_3(n,d)=0$ in order to satisfy the boundary condition that $\phi(x,y)=0$ at $y=0$ and d.

The next step is to Fourier transform interface conditions (1) and (2). The results are

$$\tilde{\phi}_1(n,b)=\tilde{\phi}_2(n,b) \tag{8a}$$

$$\tilde{\phi}_1(n,b)=\tilde{v}(n) \tag{8b}$$

$$\epsilon_r\frac{\partial\tilde{\phi}_2}{\partial y}\bigg|_{y=b}-\frac{\partial\tilde{\phi}_1}{\partial y}\bigg|_{y=b}=-\frac{\tilde{\rho}_s(n)}{\epsilon_0} \tag{8c}$$

$$\tilde{\phi}_2(n,b+h)=\tilde{\phi}_3(n,b+h) \tag{9a}$$

$$\tilde{\phi}_2(n,b+h)=\tilde{\phi}_V(n)+\tilde{\phi}_0(n) \tag{9b}$$

$$\frac{\partial\tilde{\phi}_3}{\partial y}\bigg|_{y=b+h}-\epsilon_r\frac{\partial\tilde{\phi}_2}{\partial y}\bigg|_{y=b+h}=-\frac{\tilde{\rho}(n)}{\epsilon_0} \tag{9c}$$

where $\tilde{v}$, $\tilde{\rho}_s$, $\tilde{\phi}_0$, and $\tilde{\rho}$ are unknown transformed quantities defined by

$$\tilde{v}(n)=\int_0^{L-a} v(x)\begin{Bmatrix}\cos \hat{k}_n x\\ \sin \hat{k}_n x\end{Bmatrix}dx \tag{10}$$

$$\tilde{\rho}_s(n)=\int_{L-a}^{L} \rho_s(x)\begin{Bmatrix}\cos \hat{k}_n x\\ \sin \hat{k}_n x\end{Bmatrix}dx \tag{11}$$

$$\tilde{\phi}_0(n)=\int_0^S+\int_{S+W}^{L} \phi_0(x)\begin{Bmatrix}\cos \hat{k}_n x\\ \sin \hat{k}_n x\end{Bmatrix}dx \tag{12}$$

$$\tilde{\rho}(n)=\int_S^{S+W} \rho(x)\begin{Bmatrix}\cos \hat{k}_n x\\ \sin \hat{k}_n x\end{Bmatrix}dx \tag{13}$$

and $\tilde{\phi}_V$ is the transform of the given strip potential

$$\tilde{\phi}_V(n)=\int_S^{S+W} V\begin{Bmatrix}\cos \hat{k}_n x\\ \sin \hat{k}_n x\end{Bmatrix}dx. \tag{14}$$

We will now substitute appropriate expressions in (5), (6), or (7) into (8a), (8c), (9a), and (9c) and express A_n, B_n^s, B_n^c, and C_n in terms of $\tilde{\rho}_s$ and $\tilde{\rho}$. Substituting the resulting expressions into (8b) and (9b) we obtain coupled algebraic equations

$$\tilde{G}_{11}(n)\tilde{\rho}(n)+\tilde{G}_{12}(n)\tilde{\rho}_s(n)=\tilde{\phi}_V+\tilde{\phi}_0 \tag{15a}$$

$$\tilde{G}_{21}(n)\tilde{\rho}(n)+\tilde{G}_{22}(n)\tilde{\rho}_s(n)=\tilde{v} \tag{15b}$$

where

$$\tilde{G}_{11}=\frac{1}{\det}\left[\coth \hat{k}_n h+\frac{1}{\epsilon_r}\coth \hat{k}_n b\right] \tag{16a}$$

$$\tilde{G}_{12}=\tilde{G}_{21}=\frac{1}{\det}\frac{1}{\sinh \hat{k}_n h} \tag{16b}$$

$$\tilde{G}_{22}=\frac{1}{\det}\left[\coth \hat{k}_n h+\frac{1}{\epsilon_r}\coth \hat{k}_n t\right] \tag{16c}$$

$$\det=\epsilon_0\hat{k}_n\Big[\epsilon_r+\coth \hat{k}_n h\coth \hat{k}_n b+\coth \hat{k}_n t\Big(\coth \hat{k}_n h+\frac{1}{\epsilon_r}\coth \hat{k}_n b\Big)\Big]. \tag{16d}$$

Notice that (15) contains four unknowns $\tilde{\rho}$, $\tilde{\rho}_s$, $\tilde{\phi}_0$, and $\tilde{v}$ in two equations. However, as will be described in the next section, two of the unknowns $\tilde{\phi}_0$ and $\tilde{v}$ can be eliminated in the solution process, and we can solve two equations for the two remaining unknowns $\tilde{\rho}$ and $\tilde{\rho}_s$.

Before closing this section, let us investigate the nature of the coupled algebraic equations in (15). Equations (15a) and (15b) give the Fourier transforms of potential distributions at $y=b+h$ and $y=b$, respectively. For instance, in (15a), the potential at $y=b+h$ is generated by $\tilde{\rho}$ which is located at $y=b+h$ as well as $\tilde{\rho}_s$ at $y=b$. Hence, $\tilde{G}_{12}$ contains the factor $1/\sinh \hat{k}_n h$ so that the potential due to $\tilde{\rho}_s$ becomes smaller by this factor at $y=b+h$. It is now easy to identify the physical nature of the coupling mechanism expressed by $\tilde{G}_{12}$ and $\tilde{G}_{21}$.

When $b\to 0$, $\tilde{G}_{12}=\tilde{G}_{21}\to 0$ and

$$\tilde{G}_{11}=\frac{1}{\epsilon_0\hat{k}_n\left[\coth \hat{k}_n t+\epsilon_r \coth \hat{k}_n h\right]}. \tag{17}$$

Then (15a) becomes an isolated equation corresponding to the microstripline structure. On the other hand, if $a \to 0$, the septums vanish and so does $\tilde{\rho}_s$. In this case (15a) becomes the equation for the suspended microstrip structure. In either of these two cases, the equation (15a) is an isolated (uncoupled) algebraic equation which would be derived by applying the original version of the spectral domain techniques previously reported in the literature [7]–[9] directly to the respective structures.

Actually, $\tilde{G}_{11}$, $\tilde{G}_{12}$, $\tilde{G}_{21}$, and $\tilde{G}_{22}$ correspond to the Fourier transforms of Green's functions. The first index signifies the location of y at which the function is evaluated (1 for $y=b+h$ and 2 for $y=b$) whereas the second corresponds to the location of the unit source (1 for $y=b+h$ and 2 for $y=b$). When the inverse transforms of (15) are taken, we obtain coupled integral equations in which the integrals are of convolution type. We will not go back, however, to the space domain by taking the inverse transform. Rather, we stay in the spectral domain and apply the Galerkin's method there. As we will see in the next section, such a procedure results in a small size matrix equation which is numerically easy to handle.

III. Method of Solution

The formulation in the previous section is exact. In this section, an efficient method for solving (15) will be described. This method is essentially the Galerkin's method as applied to the spectral domain formulation. From this method we can obtain line capacitances as variational quantities. Two of the unknowns $\tilde{\phi}_0$ and $\tilde{v}$ can be eliminated in the solution process and $\tilde{\rho}$ and $\tilde{\rho}_s$ will be obtained.

In the Galerkin's method, we first expand unknown $\tilde{\rho}$ and $\tilde{\rho}_s$ in terms of linear combinations of known sets of basis functions as

$$\tilde{\rho}(n)=\sum_{k=1}^{K} a_k \tilde{\rho}_k(n) \tag{18a}$$

$$\tilde{\rho}_s(n)=\sum_{m=1}^{M} b_m \tilde{\rho}_{sm}(n) \tag{18b}$$

where $a_k, k=1,2,\cdots,K$ and $b_m, m=1,\cdots,M$ are unknown coefficients. It is important that $\tilde{\rho}_k$ and $\tilde{\rho}_{sm}$ are chosen such that their inverse transform, say $\rho_k(x)$ and $\rho_{sm}(x)$ are nonzero only over the strip and septum, respectively.

We will now substitute (18) into (15a) and (15b) and take the inner product of the resulting equations with $\tilde{\rho}_i, i=1,2,\cdots,K$ and $\tilde{\rho}_{sj}, j=1,2,\cdots,M$. The results are the following coupled system of linear equations of size $(K+M)\times(K+M)$.

$$\sum_{k=1}^{K} K_{ik}^{11} a_k + \sum_{m=1}^{M} K_{im}^{12} b_m = P_i, \qquad i=1,2,\cdots,K \tag{19a}$$

$$\sum_{k=1}^{K} K_{jk}^{21} a_k + \sum_{m=1}^{M} K_{jm}^{22} b_m = 0, \qquad j=1,2,\cdots,M \tag{19b}$$

where

$$K_{ik}^{11}=\sum_{n=1}^{\infty} \tilde{\rho}_i(n)\tilde{G}_{11}(n)\tilde{\rho}_k(n) \tag{20a}$$

$$K_{im}^{12}=\sum_{n=1}^{\infty} \tilde{\rho}_i(n)\tilde{G}_{12}(n)\tilde{\rho}_{sm}(n) \tag{20b}$$

$$K_{jk}^{21}=\sum_{n=1}^{\infty} \tilde{\rho}_{sj}(n)\tilde{G}_{21}(n)\tilde{\rho}_k(n) \tag{20c}$$

$$K_{jm}^{22}=\sum_{n=1}^{\infty} \tilde{\rho}_{sj}(n)\tilde{G}_{22}(n)\tilde{\rho}_{sm}(n) \tag{20d}$$

$$\begin{aligned} P_i &= \sum_{n=1}^{\infty} \left[\tilde{\rho}_i(n)\tilde{\phi}_V(n)+\tilde{\rho}_i(n)\tilde{\phi}_0(n)\right] \\ &= \sum_{n=1}^{\infty} \tilde{\rho}_i(n)\tilde{\phi}_V(n) = \frac{L}{2}\int_0^L \rho_i(x)V\,dx \\ &= \frac{LV}{2}\int_S^{S+W} \rho_i(x)\,dx. \end{aligned} \tag{21}$$

In the derivation of (21) we have used the Parseval's relation. The terms $\tilde{\rho}_i\tilde{\phi}_0$ drop out because

$$\sum_{n=1}^{\infty} \tilde{\rho}_i\tilde{\phi}_0 = \frac{L}{2}\int_0^L \rho_i(x)\phi_0(x)\,dx = 0$$

by virtue of the fact that $\rho_i(x)=0$ for $0<x<S$ and $S+W<x<L$ whereas $\phi_0(x)=0$ for $S<x<S+W$. By the same token, the right-hand side of (19b) is also zero, and no terms containing $\tilde{v}(n)$ appear. Since P_i is now known, we can solve (19) for a_k and b_m. The line capacitance C is given by using the values of a_k when $V=1$ as

$$\frac{C}{\epsilon_0}=\sum_{k=1}^{K} a_k \int_S^{S+W} \rho_k(x)\,dx = \frac{2}{L}\sum_{k=1}^{K} a_k P_k. \tag{22}$$

It is known that the capacitance expression in (22) has a stationary nature and is free from the first-order error introduced in the choice of the basis functions $\tilde{\rho}_k(n)$ and $\tilde{\rho}_{sm}(n)$. Also, the capacitance value computed in this manner is always smaller than the true value. This fact can be advantageously used in choosing basis functions.

It is mathematically conceivable to use complete sets for $\rho_k(x)$ and $\rho_{sm}(x)$ and use their Fourier transforms as the basis functions in (19). However, such a large size matrix is not useful in practice. Much better convergence can be obtained from a small size matrix if we choose a few basis functions which represent physical characteristics of the charge distributions on the strips and septums. For instance, it is known that the charge distributions become singular toward the edges of the strips and septums. When this nature is incorporated in the choice of basis function, good results can be obtained from a very small matrix size as we will demonstrate in the next section. In selecting basis functions, it should be noted that those resulting larger capacitance values are better choices since the computed values are proven to be always smaller than the true value.

In order to obtain the characteristic impedances and the normalized guide wavelengths for even and odd modes, we need to compute the line capacitance C for the structure in Fig. 1 and the one C_{air} for the hypothetical

problem for which $\epsilon_r = 1$ in the same structure. The results are

$$Z = Z_{\text{air}}\sqrt{\frac{C_{\text{air}}}{C}} \tag{23}$$

$$\frac{\lambda_g}{\lambda} = \sqrt{\frac{C_{\text{air}}}{C}} \tag{24}$$

where $Z_{\text{air}} = 1/(cC_{\text{air}})$ with the light velocity c in free space and the free space wavelength λ.

IV. Numerical Results

Before generating reliable numerical results, it is important to select good basis functions. We have tested several different functions as $\tilde{\rho}_1(n)$ and $\tilde{\rho}_{s1}(n)$ and solved the 2×2 equations resulting from (19). For $\tilde{\rho}_1$ we tested the Fourier transforms of the following space functions

$$\rho(x) = \begin{cases} 1, & S < x < S + W \\ 0, & \text{otherwise} \end{cases} \tag{25}$$

$$\rho(x) = \begin{cases} \dfrac{4}{5W}\left[1 + \left|\dfrac{2\left(x - S - \dfrac{W}{2}\right)}{W}\right|^3\right], & S < x < S + W \\ 0, & \text{otherwise} \end{cases} \tag{26}$$

$$\rho(x) = \begin{cases} \dfrac{1}{\pi\sqrt{\left(\dfrac{W}{2}\right)^2 - \left(x - S - \dfrac{W}{2}\right)^2}}, & S < x < S + W \\ 0, & \text{otherwise.} \end{cases} \tag{27}$$

For $\tilde{\rho}_s$, we have tested

$$\rho_s(x) = \begin{cases} \dfrac{2}{a^2}(L - x), & L - a < x < L \\ 0, & \text{otherwise} \end{cases} \tag{28}$$

$$\rho_s(x) = \begin{cases} \dfrac{4}{a^4}(L - x)^3, & L - a < x < L \\ 0, & \text{otherwise} \end{cases} \tag{29}$$

$$\rho_s(x) = \begin{cases} \dfrac{1}{2a}\dfrac{L - x}{\sqrt{a^2 - (L - x)^2}}, & L - a < x < L \\ 0, & \text{otherwise.} \end{cases} \tag{30}$$

Note that the transforms of these functions can be readily obtained in closed forms.

Table I summarizes the results of various combinations of the above. Since the smaller the values of characteristic impedances the better the choice is, the combination of (27) and (30) is the most satisfactory. In (27) and (30) the singular natures of the charge distribution near the edges of the strip and septum are included, and, hence, they represent actual distribution most faithfully. It is also noted that the proper choice of the $\tilde{\rho}_s$ function is more effective in accurate calculation of even-mode impedance whereas that of $\tilde{\rho}$ is more important for odd-mode impedance. These findings are in agreement with the physical behavior of the potential and charge distributions. For the even-mode impedance, the electric fluxes originate at the strip and terminate at the grounded conductor as the potentials of the two strips are identical. Hence, there is a strong charge concentration toward the edges of the septums. The inclusion of singularity in ρ_s correctly represents this phenomenon. On the other hand, for the odd-mode, most of the fluxes are between two strips as their potentials are opposite in polarity. The singular nature at the edges of strips, therefore, improves the numerical results.

We have also studied the convergence of the solution by increasing the matrix size from 2×2 to 4×4. In the 4×4 case, (26) and (27) were used for $\tilde{\rho}_1$ and $\tilde{\rho}_2$ whereas (29) and (30) for $\tilde{\rho}_{s1}$ and $\tilde{\rho}_{s2}$. The results are given in Table I. As the convergence is seen to be very good, we concluded that it was unjustified to use any larger size matrix with increasing computation time. All the data reported in the rest of the paper were generated by the use of a 4×4 matrix. Accuracy can be improved further by the use of a larger size matrix. However, the degree of improvement becomes increasingly small, and, hence, such improvement is economically unjustified. The error of the numerical results reported here is believed to be less than 2

TABLE I
Comparison of the Computed Results for Different Choices of Basis Functions

Combinations		Characteristic Impedances	
ρ	ρ_s	Even Mode	Odd Mode
25	28	162.43	43.20
26	29	152.33	42.70
26	30	147.82	42.45
27	30	146.61	40.26
(4 x 4 matrix		145.52	39.92)*

$\epsilon_r = 9.6$, $S/h = 0.15$, $W/h = 1.2$, $a/h = 7.0$, $b/h = 10.0$, $t/h = 10.0$, $L/h = 10.0$.

*(26) and (27) are used as $\rho_i, i = 1,2$, and (29) and (30) as ρ_{sj}, $j = 1,2$.

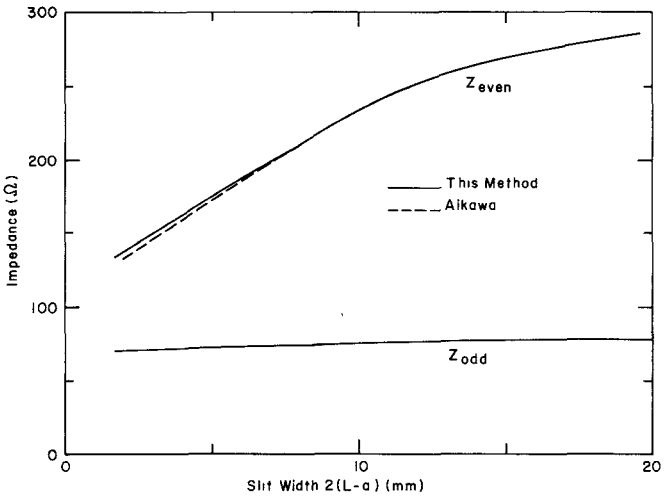

Fig. 2. Comparison of computed characteristic impedances with those by Aikawa. $\epsilon_r = 2.4$, $S = 0.335$ mm, $W = 1.48$ mm, $L = 16.4$ mm, $t = 16.4$ mm, $h = 1.64$ mm, $b = 8.2$ mm

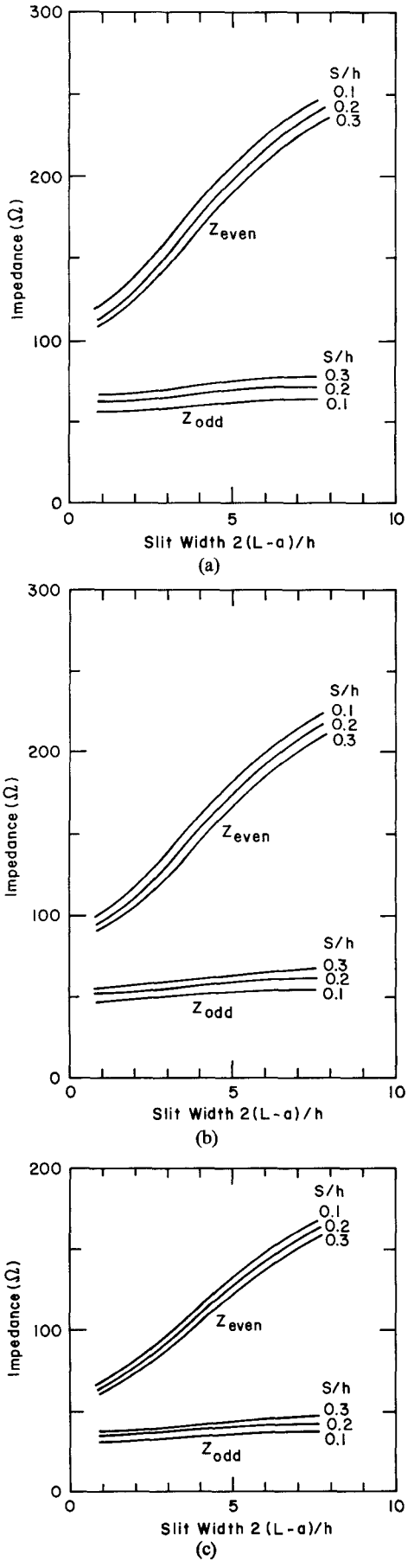

Fig. 3. Characteristic impedances of coupled suspended lines versus the slit width. $W/h=1.2$, $L/h=b/h=t/h=10.0$. (a) $\epsilon_r=2.4$. (b) $\epsilon_r=3.8$. (c) $\epsilon_r=9.6$.

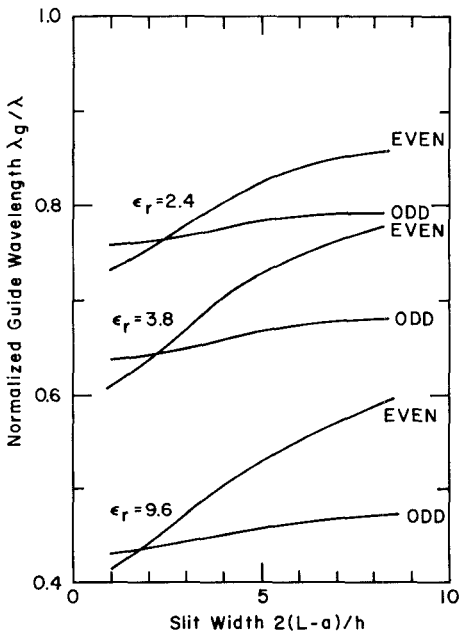

Fig. 4. Normalized guide wavelength versus the slit width. $W/h=1.2$, $L/h=b/h=t/h=10.0$, $S/h=0.2$

percent from the past experience gained in applying the spectral domain method to microstripline problems.

In Fig. 2, we compared our results with those reported by Aikawa [1]. The slit width is meant to be the distance between edges of two septums. Except for the characteristic impedance of the even mode of the structure with small slit width (large septums), the results are indistinguishable on the graph. It is noted that Aikawa used the finite difference technique in which finer mesh points for accelerating the convergence of computation have been used only in the region surrounding the strips [1], [2]. No such procedures seemed to have been implemented near the edges of the septum. It is believed that the results so obtained are accurate for the odd mode since the strong interaction between strips can be taken into account correctly. However, in the even-mode case, the interaction between the strip and septum becomes more important, and, hence, finer mesh points near the septum edges are felt necessary.

In Fig. 3, characteristic impedances of even and odd modes are plotted versus the slit width for a number of structural parameters. Throughout Figs. 2 and 3 it is clear that the even-mode impedance can be tuned over a wide range by changing the septum size whereas the odd-mode impedance is virtually unaffected.

Fig. 4 shows the guide wavelength λ_g normalized by the free space wavelength λ versus the slit width. It is clearly seen that the guide wavelength of the even mode vaires in a wider range than that of the odd mode. Also notice that at certain values of the septum width the guide wavelengths of even and odd mode coincide. This phenomenon is useful for the directional coupler applications as pointed by Aikawa [2].

Variations of characteristic impedances and guide wavelengths versus the strip width are shown in Fig. 5 for a number of different dielectric materials. Characteristic

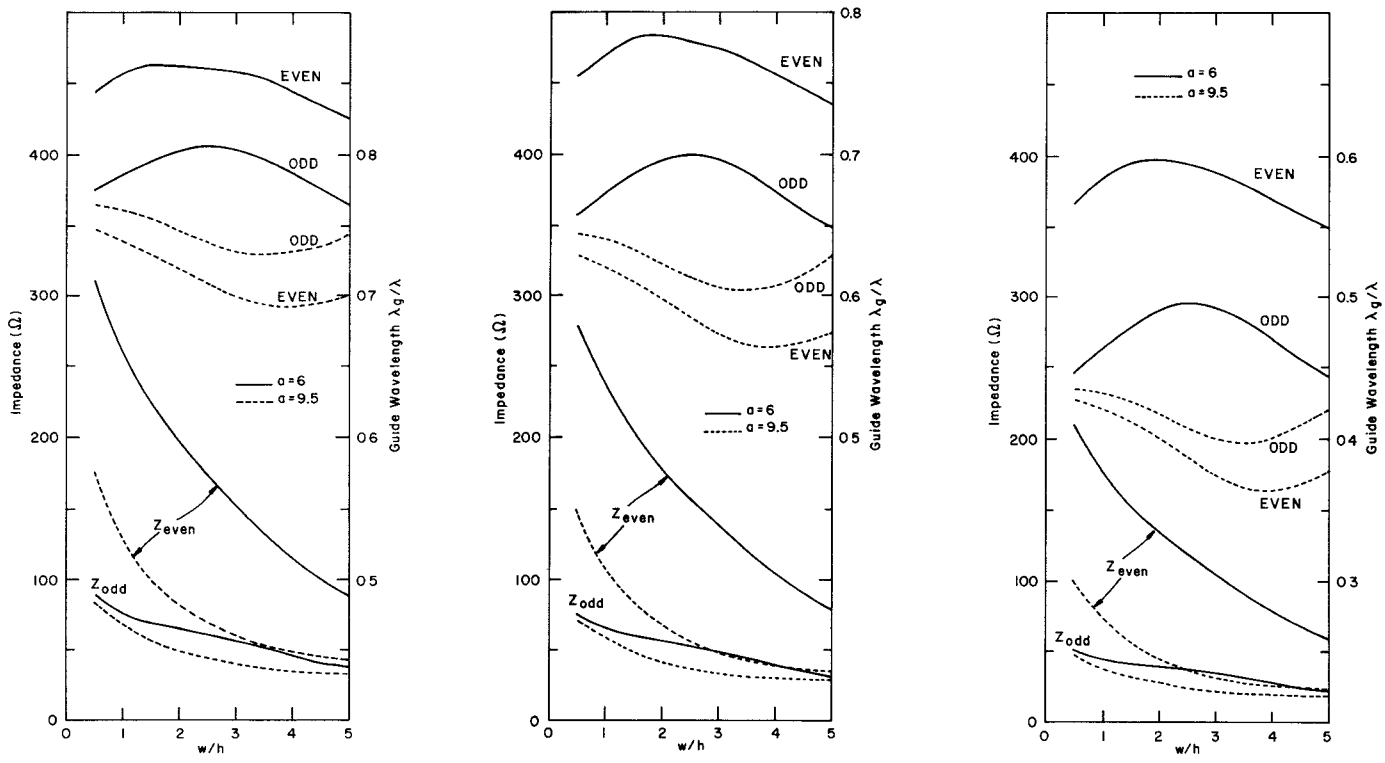

Fig. 5. Characteristic impedance and normalized guide wavelength versus strip width. $L/h=b/h=t/h=10.0$, $S/h=0.2$. (a) $\epsilon_r=2.4$. (b) $\epsilon_r=3.8$. (c) $\epsilon_r=9.6$.

impedances of the even mode vary more rapidly with the strip width than those of the odd mode. Two values of a, the septum width, are chosen. For one choice of a, the guide wavelength of the even mode is larger than that of the odd mode for any strip width in the range computed. For another choice, the situation is completely opposite.

V. Conclusions

In this paper we presented a new efficient method for computing the characteristic impedance and the guide wavelength in coupled suspended microstriplines with tuning septums. The method has a number of advantages over many other methods and, in addition, is quite general so that it can be applied to many similar structures. The accuracy of the results was compared with available data. A number of numerical data have been generated.

The structure considered here is believed useful in microwave integrated circuit applications for such devices as a quadrature hybrid. In addition, we conjecture that the structure can be used as a transition from one type of transmission line to another, such as microstrip to coplanar and microstrip to dielectric waveguide [10]. This is because in the present structure we have greater flexibility in controlling the field distributions in the cross section due to the presence of the septums than in many other transition structures. The work along this line will be attempted in the future.

The computation time in the case of a 4×4 matrix was 1/s (CPU time) per point on a DECSYSTEM-10 computer.

References

[1] M. Aikawa, "Wide-band strip-line reverse-phase hybrid ring in GHz band," *Electronics and Communications in Japan*, vol. 58-B, no. 10, pp. 521–528, Oct. 1975.

[2] ——, "Microstrip line directional coupler with tight coupling and high directivity," *Electronics and Communications in Japan*, vol. J60-B, no. 4, pp. 253–259, Apr. 1977.

[3] B. Sheleg and B. E. Spielman, "Broadband directional couplers using microstrip with dielectric overlays," *IEEE Trans. Microwave Theory Tech.*, vol. MTT-22, pp. 1216–1220, Dec. 1974.

[4] A. Podell, "A high directivity microstrip coupler technique," in *IEEE Int. Microwave Symp.* (Newport Beach, CA), May 1970, pp. 33–36.

[5] J. Lange, "Interdigitate stripline quadrature hybrid," *IEEE Trans. Microwave Theory Tech.*, vol. MTT-17, pp. 1150–1151, Dec. 1969.

[6] M. V. Schneider and W. W. Snell, Jr., "Harmonically pumped stripline down converter," *IEEE Trans. Microwave Theory Tech.*, vol. MTT-23, pp. 271–275, Mar. 1975.

[7] T. Itoh and R. Mittra, "Dispersion characteristics of the slot lines," *Electron. Lett.*, vol. 7, no. 13, pp. 364–365, Jul. 1971.

[8] ——, "A technique for computing dispersion characteristics of shielded microstrip lines," *IEEE Trans. Microwave Theory Tech.*, vol. MTT-22, pp. 896–898, Oct. 1974.

[9] T. Itoh, "Analysis of microstrip resonators," *IEEE Trans. Microwave Theory Tech.*, vol. MTT-22, pp. 946–952, Nov. 1974.

[10] ——, "Inverted strip dielectric waveguide for millimeter-wave integrated circuits," *IEEE Trans. Microwave Theory Tech.*, vol. MTT-24, pp. 821–827, Nov. 1976.